Multi-scale modeling of urban air pollution: development and application of a Street-in-Grid model by coupling MUNICH and Polair3D

Youngseob Kim[1], You Wu[2], Christian Seigneur[1], and Yelva Roustan[1]

[1]CEREA, Joint Laboratory École des Ponts ParisTech / EDF R&D, Université Paris-Est, 77455 Champs-sur-Marne, France
[2]EDF R&D China, 100005 Beijing, China

Correspondence to: Youngseob Kim (youngseob.kim@enpc.fr)

Abstract. A new multi-scale model of urban air pollution is presented. This model combines a chemical-transport model (CTM) that includes a comprehensive treatment of atmospheric chemistry and transport at spatial scales down to 1 km and a street-network model that describes the atmospheric concentrations of pollutants in an urban street network. The street-network model is the Model of Urban Network of Intersecting Canyons and Highways (MUNICH), which consists of two
5   main components: a street-canyon component and a street-intersection component. MUNICH is coupled to the Polair3D CTM of the Polyphemus air quality modeling platform to constitute a Street-in-Grid (SinG) model. MUNICH is used to simulate the concentrations of the chemical species in the urban canopy, which is located in the lowest layer of Polair3D, and the simulation of pollutant concentrations above roof-tops is performed by Polair3D. Interactions between MUNICH and Polair3D occur at roof level and depend on a vertical mass transfer coefficient that is a function of atmospheric turbulence. SinG is
10 used to simulate the concentrations of nitrogen oxides (NO_x) and ozone (O_3) in a Paris suburb. Simulated concentrations are compared to NO_x concentrations measured at two monitoring stations within a street canyon. SinG shows better performance than MUNICH for nitrogen dioxide (NO_2) concentrations. However, both SinG and MUNICH underestimate NO_x. Model performance for NO_x concentrations is not sensitive to using a complex chemistry model in MUNICH and the Leighton $NO/NO_2/O_3$ set of reactions is sufficient.

15 # 1   Introduction

Urban air pollution has been a public health issue for many decades. Historically, the first urban air quality model with spatial and temporal resolution was developed for the Los Angeles basin in California, USA (Reynolds et al., 1973). This three-dimensional (3D) gridded Eulerian model used the atmospheric diffusion (mass-conserving) equation to calculate the change with respect to time of the relevant air pollutant concentrations due to emissions, transport, chemical transformation, and
20 deposition. Because of the urban design of western U.S. cities, there was no need to take buildings into account explicitly.

European cities differ from the Los Angeles basin because of the presence of densely built districts with street-canyon configurations. Consequently, although air quality models such as the one initially used for the Los Angeles basin are commonly used to calculate urban background pollution, different types of air quality models are needed to calculate air pollution at the

street scale. The conceptual approach of the Operational Street Pollution Model (OSPM) has typically been used (Berkowicz, 2000). The air pollutant concentrations are calculated within a street-canyon assuming uniform traffic emissions across the street-canyon, but air pollutant concentrations can be calculated in ventilated and recirculated zones of the street-canyon. Mass transfer between the street and the urban background atmosphere at the top of the street (i.e., roof level) is simulated.

5   This initial concept has been extended to calculate air pollutant concentrations within a network of streets with the SIRANE model (Soulhac et al., 2011). Although the SIRANE formulation does not distinguish recirculation and ventilation zones and assumes a uniform concentration for each street segment, it provides a significantly better treatment of pollutant transport across street intersections. The development of the SIRANE formulation is based on a comprehensive investigation of airflow and mass transfer via wind tunnel experiments and computational fluid dynamics (CFD) simulations. SIRANE has been applied

10   to various urban districts and has shown satisfactory performance when compared to ambient air pollutant concentrations (e.g. Soulhac et al., 2012). However, the treatment of the urban background above roof level in SIRANE is modeled using a Gaussian model formulation, which prevents the use of a comprehensive atmospheric chemistry. Consequently, it is not appropriate to simulate secondary air pollutants such as ozone (O_3) or fine particulate matter ($PM_{2.5}$), which require modeling the formation of secondary pollutants with a comprehensive chemical kinetic mechanism.

15   Therefore, there is a dire need to combine the advantages of 3D gridded Eulerian models, which can simulate urban background concentrations of all major air pollutants of interest, and those of street-network models, which can simulate the concentrations of air pollutants in complex urban canopy configurations. The multi-scale combination of Eulerian models with near-source models was developed initially for the treatment of plumes from tall stacks in the Los Angeles basin (Seigneur et al., 1983). Many other "Plume-in-Grid" (PinG) models have been developed over the following three decades (see Karam-

20   chandani et al., 2011, for an overview). Later PinG model development efforts have included PinG models for line sources, area sources, and volume sources using various modeling approaches (e.g., Cariolle et al., 2009; Karamchandani et al., 2009; Huszar et al., 2010; Jacobson et al., 2011; Briant and Seigneur, 2013; Holmes et al., 2014; Kim et al., 2014) in order to treat aircraft emissions, ship emissions, traffic emissions from roadways, and fugitive emissions from industrial sites. However, there is currently no integrated model that dynamically combines an Eulerian model with a street-network model. The objective of

25   this work is to develop the formulation of such a Street-in-Grid model (SinG), fully consistent with the mass conservation principle, and present its initial application to an actual urban case study. The Eulerian host model selected for this work is Polair3D of the Polyphemus air quality modeling platform (Mallet et al., 2007), a 3D chemical-transport model (CTM), which has been widely applied in Europe, North America, South America, Asia, and Africa (e.g., Sartelet et al., 2012). The Model of Urban Network of Intersecting Canyons and Highways (MUNICH), which is used to simulate subgrid concentrations in the

30   urban canopy represented by the street network, is presented in the next section. Then, the coupling of MUNICH to Polair3D is described in Section 3. Finally, some initial applications of MUNICH and the SinG model to a Paris suburb are discussed.

2 Description of MUNICH

MUNICH is based conceptually on the SIRANE general formulation (Soulhac et al., 2011). We can distinguish two main components to MUNICH: (1) the street-canyon component, which represents the atmospheric processes in the volume of the urban canopy, and (2) the street-intersection component, which represents the processes in the volume of the intersection.

5 These components are connected to the Polair3D model at roof level and are also interconnected. We describe each one of these components in turn.

2.1 Street-canyon component

For a street segment, which is defined as a street component bounded by intersections with other streets at each end, the following assumptions are used (Soulhac et al., 2011):

10   – Air pollutant concentrations are uniform within a street segment.

   – The width of the street and the height of the buildings are uniform.

   – Emissions of air pollutants and deposition of air pollutants are uniform along the street segment. However, deposition fluxes to different surfaces, including pavement, building walls, and roofs are distinguished using the urban dry deposition model of Cherin et al. (2015).

15   – The wind direction follows the street segment direction.

   – The wind speed is uniform and is related to the wind speed at roof level, the angle between the wind direction at roof level and the street segment direction, and the street segment characteristics (width and height).

   – Steady state is assumed for a given time step.

Assuming steady state, the mass flux (Q in $\mu g\,s^{-1}$) balance is applied to calculate the concentration of an air pollutant in a

20 street segment.

$$Q_\mathrm{s} + Q_\mathrm{inflow} + Q_\mathrm{chem} \;=\; Q_\mathrm{vert} + Q_\mathrm{outflow} + Q_\mathrm{dep} \qquad (1)$$

where Q_s is the source emission rate, Q_inflow is the inflow rate of the air pollutant entering the street from upwind (typically via an intersection), Q_vert is the vertical flux by turbulent diffusion at roof level (see Section 2.1.1), Q_outflow is the outflow rate of the air pollutant leaving the street in the downwind direction, Q_dep is the pollutant loss rate due to atmospheric deposition, and Q_chem

25 is the air pollutant chemical transformation rate (positive for formation and negative for destruction). The emission term, Q_s, is obtained typically from a traffic emission model. The inflow term, Q_inflow, is obtained from the street-intersection component (see Section 2.2). The outflow rate, Q_outflow is calculated as follows:

$$Q_\mathrm{outflow} \;=\; HW u_\mathrm{street} C_\mathrm{street} \qquad (2)$$

where H is the mean building height in the street segment and W is the mean street width, u_street is the mean horizontal wind

30 velocity in the street segment (see Section 2.1.2), and C_street is the air pollutant concentration in the street segment.

2.1.1 Turbulent vertical mass transfer at the top of the street segment

The vertical flux, Q_{vert}, as formulated in SIRANE does not depend on the building height in the street segment and is, therefore, defined by the external flow condition, based on Salizzoni et al. (2009).

$$Q_{\text{vert}} = \frac{\sigma_{\text{w}} W L}{\sqrt{2\pi}} \left(C_{\text{street}} - C_{\text{background}} \right) \tag{3}$$

5 where $C_{\text{background}}$ is the mean concentration above the street segment, L is the street length, and σ_{w} is the standard deviation of the vertical wind velocity at roof level, which depends on atmospheric stability. One notes that this approach represents the turbulent mass transfer rate using a mass transfer coefficient with unit of a velocity. Such an approach is routinely used in engineering where mass transfer coefficients are empirically defined and combined with concentration gradients to calculate mass transfer rates. In air quality modeling, this approach is also used to model dry deposition and turbulent mass transfer in
10 the surface layer is typically approximated with a deposition velocity.

A slightly different parametrization was recently proposed by Schulte et al. (2015) who used a turbulent dispersion coefficient defined as follows:

$$K_m = \sigma_{\text{w}} l \tag{4}$$

where l is a characteristic mixing length within the street-canyon. By assuming that the size of the large turbulent eddies
15 dominating vertical mixing is limited by the smaller size of the street width and height, l is proportional to the smaller of W and H as follows.

$$\frac{1}{l} \sim \left(\frac{1}{W} + \frac{1}{H} \right) \tag{5}$$

Then

$$l = \beta_1 \frac{W H}{W + H} = \beta_1 H \frac{1}{1 + a_r} \tag{6}$$

20 where β_1 is a constant and a_r is the aspect ratio (ratio of building height to street width, H/W) (Landsberg, 1981).

Then, the vertical flux at roof level is expressed using the turbulent dispersion coefficient as follows:

$$Q_{\text{vert}} = \beta_2 K_m \frac{W L}{H} \left(C_{\text{street}} - C_{\text{background}} \right) \tag{7}$$

By combing Equation 7 with Equations 4 and 6, we obtain

$$Q_{\text{vert}} = \beta \sigma_{\text{w}} W L \left(\frac{1}{1 + a_r} \right) \left(C_{\text{street}} - C_{\text{background}} \right) \tag{8}$$

25 where $\beta = \beta_1 \beta_2$.

The constant β can be estimated by comparison to Equation 3. Because the vertical flux in Equation 3 is estimated using the unity aspect ratio ($a_r = 1$), we assume that the computed vertical fluxes with Equations 3 and 8 are equal when $a_r = 1$. We obtain $\beta = 0.45$. Figure 1 compares the vertical transfer coefficient estimated with Equations 3 and 8. If $a_r < 1$, i.e., in an area with low buildings, then the transfer coefficient is greater with the formulation of Schulte et al. (2015) than that of
30 SIRANE. On the contrary, if $a_r > 1$, i.e., in a street-canyon configuration, then the vertical transfer is reduced compared to that of SIRANE.

Geoscientific
Model Development
Discussions
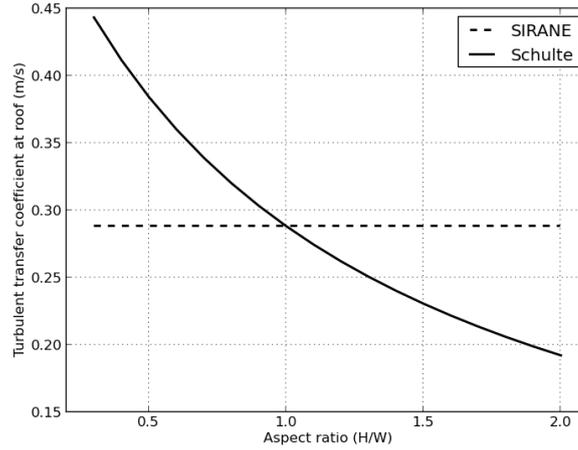
Figure 1. Comparison of the turbulent transfer coefficients of the SIRANE formulation (dotted line) and the formulation of Schulte et al. (2015) (solid line).

2.1.2 Mean wind velocity within the street-canyon

Here, we use the exponential wind vertical profile proposed by Lemonsu et al. (2004) and used by Cherin et al. (2015) in their modeling of dry deposition within street-canyons. The corresponding formulas were modified here to be specific to the angle between the wind direction and the street-canyon direction (Lemonsu et al., 2004 and Cherin et al., 2015 averaged the wind profile over all possible angles).

– For narrow canyons, $a_r > 2/3$:

$$u_{\text{street}} = \frac{2}{\pi} u_H cos(\varphi) exp\left(\frac{a_r}{2}\left(\frac{z}{H}-1\right)\right) \tag{9}$$

where φ is the angle between the wind direction above roof level and the street direction. u_H is the wind speed at the building height and is a function of the friction velocity.

– For the so-called intermediate case (i.e., moderate canyons), $1/3 \leq a_r \leq 2/3$:

$$u_{\text{street}} = \left[1 + 3\left(\frac{2}{\pi}-1\right)\left(\frac{H}{W}-\frac{1}{3}\right)\right] u_H cos(\varphi) exp\left(\frac{a_r}{2}\left(\frac{z}{H}-1\right)\right) \tag{10}$$

– For a wide configuration, $a_r < 1/3$:

$$u_{\text{street}} = u_H cos(\varphi) exp\left(\frac{a_r}{2}\left(\frac{z}{H}-1\right)\right) \tag{11}$$

An average wind speed can be derived from these empirical wind profiles by integrating over the entire street-canyon height ($0 < z < H$). These empirical wind profiles are exponential functions and are, therefore, qualitatively similar to the profile used in SIRANE (Soulhac et al., 2008) to derive the average wind velocity within the street-canyon. The wind speeds calculated

using these wind profiles and those in SIRANE are compared in Figure 2. This figure illustrates the differences in the mean wind speed obtained for different values of the aspect ratio ranging from 0.1 to 2. The largest differences are obtained when $a_r = 2/3$ and the angle between the wind direction and the street direction is lower. For $\varphi = 0$, the average wind speed of MUNICH is about 2/3 that of SIRANE.

(a) 0°

(b) 30°

(c) 60°
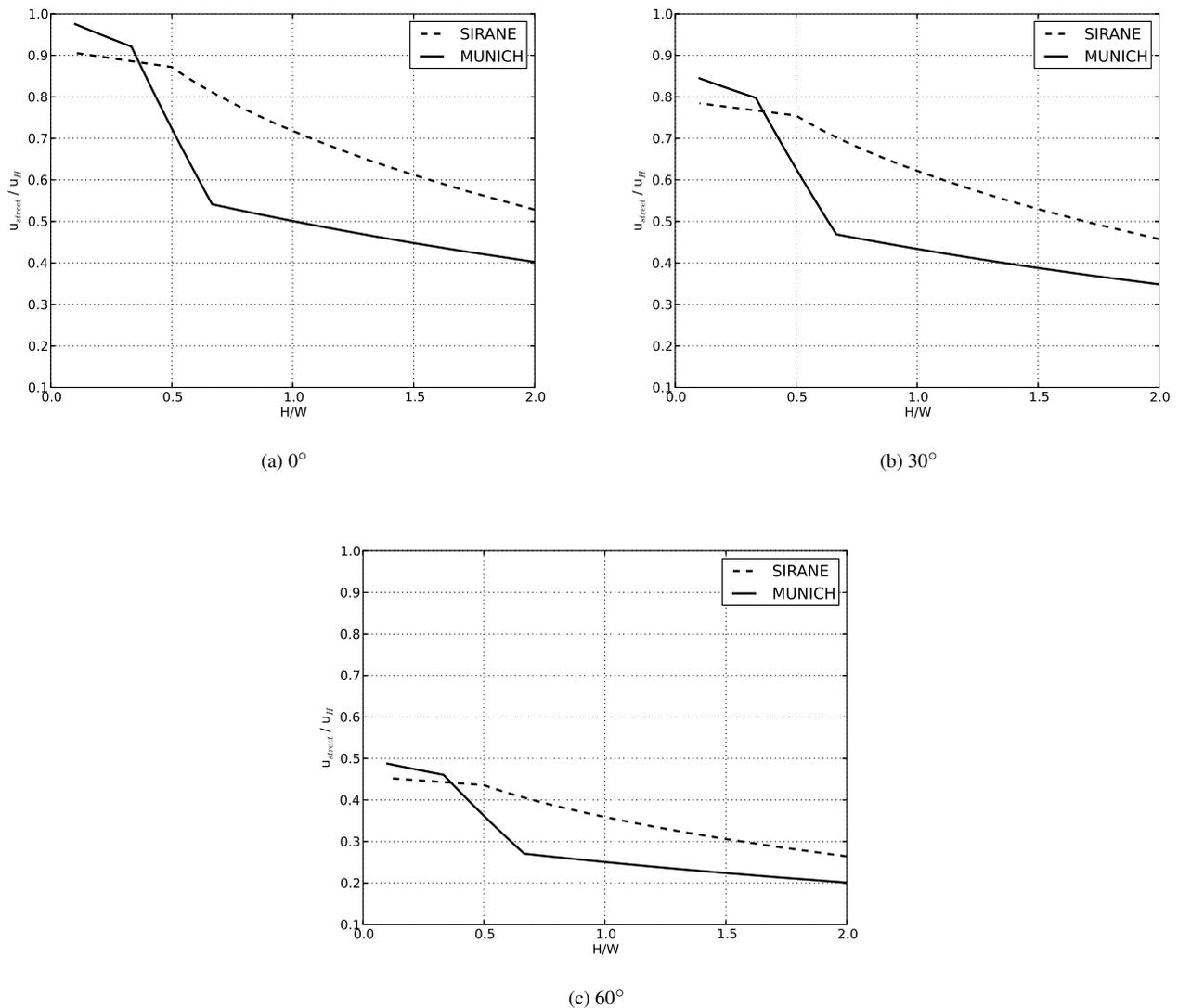
Figure 2. Comparison of the mean horizontal wind velocity (normalized with respect to the wind speed at roof level) within the street-canyon calculated with the profiles of SIRANE (Soulhac et al., 2008) (dotted lines) and MUNICH (Lemonsu et al., 2004) (solid lines) as a function of the street aspect ratio for three different angles between the wind direction and the street direction (a) 0°, (b) 30°, (c) 60°

2.2 Street-intersection component

The street-intersection component of MUNICH involves the following assumptions, also used in SIRANE (Soulhac et al., 2009):

- The air pollutant concentration is not uniform across the intersection (as it has sometimes been assumed in earlier work).
5
- The advective air flow in the street network is compensated by inflow or outflow at the top (roof level) of the intersection to ensure mass balance.
- The mean air flow follows the wind direction at roof level.
- The streamlines of the flow from a street to other streets across the intersection cannot cross one another.
- Fluctuations in wind direction are taken into account when constructing the air flows from one street to others across the
10   intersection.

Accordingly, the air mass fluxes (and the associated pollutant mass fluxes) are computed for the streets that are connected to the intersection (entering or leaving the intersection) using Equation 1. The air mass fluxes for the streets are corrected by the computed vertical air flux in the intersection at roof level.

If one considers only the mean air flow, the air flow rates for the streets are determined solely based on the configuration
15 of the streets, their intersection and the wind direction above roof level. However, experiments in a wind tunnel and CFD simulations have shown that fluctuations in wind direction influence significantly the air flow across an intersection (Soulhac et al., 2009). Accordingly, one must take into account these fluctuations to properly account for the transfer of air (and pollutant) mass across the intersection. Then, the computation of the air fluxes depends not only on the mean wind direction, but also on the wind fluctuation. The wind direction is assumed to follow a Gaussian distribution centered on its mean value.

20 ## 2.3 Chemical reactions

In MUNICH, the CB05 chemical kinetic mechanism (Yarwood et al., 2005) is implemented to ensure consistency with Polair3D in the SinG configuration. CB05 consists of 53 species including volatile organic compounds (VOC) and inorganic species and 155 chemical reactions including 23 photolyses. However, nitric oxide (NO) emissions in the urban canopy are likely to scavenge O_3 and other oxidants, thereby suppressing VOC chemistry. Accordingly, a simple three-reaction mechanism
25 involving solely NO, nitrogen dioxide (NO_2) and O_3, known as the Leighton photostationary state (Leighton, 1961), was also implemented. These two mechanisms are compared below in terms of model performance and computational costs.

2.4 Dry and wet deposition

Dry deposition is computed using the approach developed for an urban canopy (Cherin et al., 2015). Surfaces available for dry deposition include pavement (street and sidewalks), building walls, and building roofs. The dry deposition fluxes (in
30 $\mu g \, m^{-2} \, s^{-1}$) are calculated by multiplying the pollutant concentrations (in $\mu g \, m^{-3}$) and the pollutant deposition velocities (in $m \, s^{-1}$). The estimation of the deposition velocities depends on the atmospheric conditions and the surface properties, which

differ among the surface types. For the building roofs, the background concentrations over the urban canopy are used, whereas the concentrations within the street network are used for the pavement and building walls.

Wet deposition consists of the scavenging by precipitation and deposition to pavement and building roofs. Wet deposition to the building roofs is estimated by the precipitation intensity and the background concentrations over the urban canopy. The scavenging and deposition to the pavement is computed for the entire atmospheric column and includes both the background concentrations above roof tops and the concentrations within the urban canopy:

$$F_{\text{street}} = \Lambda \left(C_{\text{street}} H + C_{\text{background}} (z_c - H) \right) \tag{12}$$

where F_{street} is the wet deposition flux to the pavement ($\mu g \, m^{-2} \, s^{-1}$), Λ is the scavenging coefficient (s^{-1}), and z_c is the cloud base height (m). The in-cloud wet scavenging is supposed to have a weak impact for the species considered here.

## 3 Coupling of MUNICH with Polair3D: Street-in-Grid model

We describe here a new model, "Street-in-Grid" (SinG), which combines the MUNICH street-network model and the Polair3D CTM. SinG is conceived to conduct a multi-scale simulation, which estimates both grid-averaged concentrations at the urban scale and concentrations within each street segment. This combined model provides the following advantages.

- It allows one to estimate the influence of the background concentrations on the concentrations within the street network and vice-versa.

- There is no double counting of emissions, originating within the urban canopy: these emissions are input data to MUNICH and, therefore, they are removed from the grid-averaged emission inventory of Polair3D.

- There is consistency between the treatment of physical and chemical processes at different scales. Transport and dispersion of pollutants at the urban and street-network scales are calculated from the same meteorological data. Similarly, the same chemical mechanism and the same formulations for dry and wet atmospheric deposition are used at those different scales. There is, however, the option to use a reduced form of the chemical mechanism within the street network, following Karamchandani et al. (1998).

Figure 3 shows schematically the concept of the SinG model. As MUNICH is located within the lowest Polair3D layer, meteorological variables in that layer, such as wind speed and direction, are transferred to MUNICH via the SinG interface. Air pollutant concentrations in the Polair3D lowest layer are also transferred since they are used as the background concentrations for the street network. Then, MUNICH computes the mass fluxes between the urban canopy (i.e., the street network) and the urban atmosphere above roof level and the SinG interface transfers them to Polair3D to compute new air pollutant concentrations in the grid cells above the urban canopy.

The interfacing between MUNICH and Polair3D is conducted at fixed time steps, which were set at 10 min in the following application.
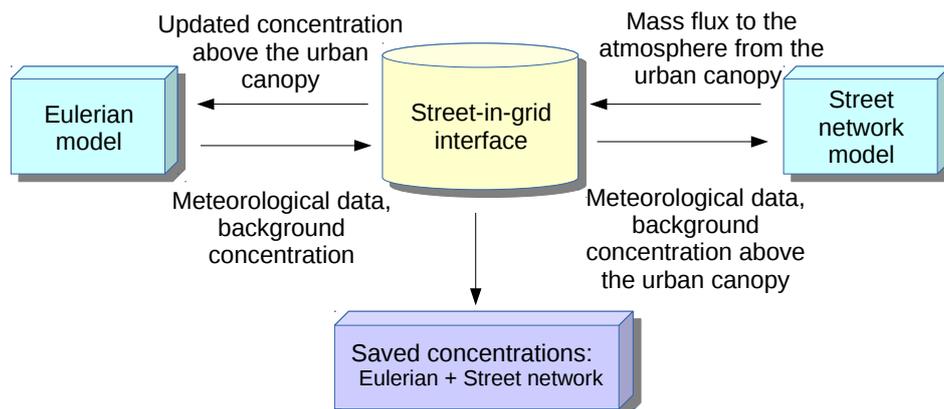
Figure 3. Schematic diagram of the Street-in-Grid model.

4 Application of MUNICH to a street network in a Paris suburb

4.1 Simulation domain and setup

MUNICH was applied to simulate the concentrations of pollutants in a Paris suburb (Le Perreux-sur-Marne, 13 km east of
Paris). Simulations for gas-phase species including NO_x were conducted during the period from March 24 to June 14, 2014.
5   Figure 4 displays the location of the modeling domain.

4.2 Traffic emissions

The traffic emissions for the simulation domain were estimated using the dynamic traffic model, Symuvia (Leclercq et al.,
2007) with the COPERT 4 emission factors (http://emisia.com/products/copert-4/versions), as part of the TrafiPollu project
(http://www.agence-nationale-recherche.fr/?Project=ANR-12-VBDU-0002). The emission rates depend on the vehicle speed
10   and composition of the fleet. Two typical days (March 25 for weekday and March 30 for weekend) were chosen for the traffic
simulation.

    The dynamic traffic model estimates the emission rates for each traffic direction of a two-way street. The traffic emissions
of a two-way street were merged to obtain one emission rate for the street segment. Surface areas of intersections are not taken
explicitly into account in MUNICH and streets are connected at the center of the intersection, i.e., an intersection is represented
15   by a point using a latitude/longitude coordinate set. In this work, the traffic emissions were prepared for 577 street segments
The obtained emission data for the street network are presented in Figure 5.

4.3 Geographic data

Traffic lane widths and building heights were obtained from the BD TOPO database (http://professionnels.ign.fr/bdtopo). Total street width includes the lane width, the sidewalk width or the highway shoulder width (the A86 highway passes through the modeling domain). For minor surface roads, a width of 3 m was used for sidewalks by default, which corresponds to

5 2 sidewalks (the minimum sidewalk width in France is 1.4 m). For the A86 highway, 20 m were added to the lane width including 2 shoulders (4 m), a median strip (1.5 m), and 2 urban-train lanes (4 m). Street widths and building heights of the 15 major streets were explicitly estimated. For the other streets, average street width (7.5 m) and building height (6.9 m) estimated for the modeling domain were used.

4.4 Meteorological data

10 Meteorological data, including wind direction/speed, planetary boundary layer (PBL) height, and friction velocity, were obtained from a Weather Research and Forecasting (WRF) model (Skamarock et al., 2008) simulation counducted with a horizontal resolution of $1.5 \times 1.5\,\mathrm{km}^2$ (Thouron et al., 2017). The simulated meteorological data were compared to the measurements at urban-background meteorological stations near the simulation domain and showed satisfactory results.
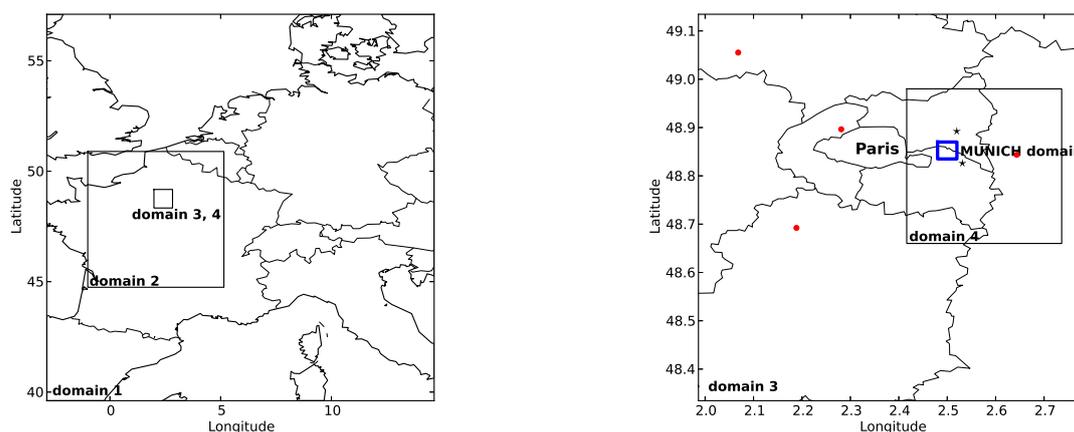
Figure 4. Modeling domains for the Street-in-Grid simulations. In the right panel, the blue box corresponds to the modeling area in suburban Paris for the MUNICH simulations. The black stars and red circles show the locations of the urban background air monitoring stations. SinG is only used for domain 4. Measured data at the stations with the black stars are used for background concentrations in the MUNICH simulations

4.5   Background concentrations

Background concentrations of NO, NO$_2$, and O$_3$ were obtained from two urban background air monitoring stations near the modeling area (5 to 7 km from the area, see Figure 4). Averaged values of the hourly measured concentrations at the two stations were used to compute the vertical mass transfer at the top of the street network in Equations 3 and 8. These stations

5 are operated by AIRPARIF, the air quality agency of the Paris region (http://www.airparif.asso.fr/).

4.6   Results

Figure 6 shows that simulated concentrations of NO$_x$ are high in the streets where the emission rates are high (see Figure 5). The concentrations of NO$_x$ during nighttime on March 25 reach 160 μg m^{-3} over the major streets. During the morning rush-hour on the same day, the concentrations of NO$_x$ increase to 600 μg m^{-3}. The modeled high concentrations during the rush-hour

10 are due not only to high emission rates but also to stable meteorological conditions with low PBL height (520 m) and wind speed (2.5 m/s). One notes that there is a clear difference between the spatial patterns of the emission maps (Figure 5) and concentration maps (Figure 6). Streets with no or little NO$_x$ emissions display non-negligible NO$_x$ concentrations, thereby highlighting the importance of advective and turbulent transport in the street network.

(a) Nighttime　　　　　　　　　(b) Morning rush-hour
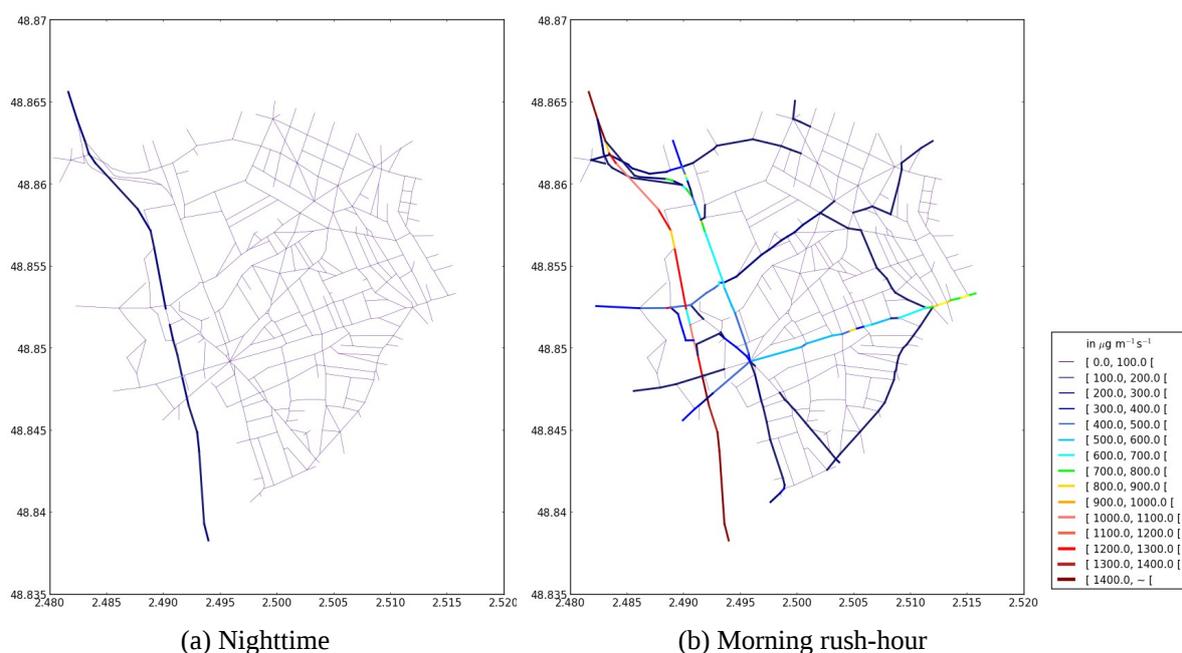
Figure 5. NO$_x$ emission rates (μg m^{-1} s^{-1}) used in MUNICH simulations for a week day (a) during nighttime at 1 AM (UTC) (b) in the morning rush-hour at 7 AM (UTC) on March 25, 2014.

Figure 7 compares the modeled 24-h averaged concentrations of NO_2 with the concentrations measured at the air monitoring stations operated by AIRPARIF during the TrafiPollu project on the two sidewalks of Boulevard Alsace-Lorraine for the period from April 6 to June 15. Statistical indicators defined in Appendix A for the comparison of hourly concentrations are provided in Table 1. The NO_2 modeled concentrations using MUNICH generally underestimate the observations with a mean negative

5 bias of 32%. It is not obvious to attribute these discrepancies in NO_2 simulations to the model formulation or the input data (background concentrations, meteorological data and emission data from the dynamic traffic model). Nevertheless the sensitivity to the choice of the background concentration is important. The background concentrations are estimated using the mean of concentrations measured at two urban background stations (see Figure 4). Figure 8 shows similar temporal evolution in the measured NO_2 and NO_x daily concentrations between the two stations. However significant discrepancies in their

10 pick values are observed (up to a maximum difference of 300% in the hourly concentrations). It implies that the measured background concentrations certainly do not always correspond to the concentration above a given street. This result points out the difficulty of identifying measurements that are truly representative of the "urban background" as wished in the street-


(a) Nighttime   (b) Morning rush-hour
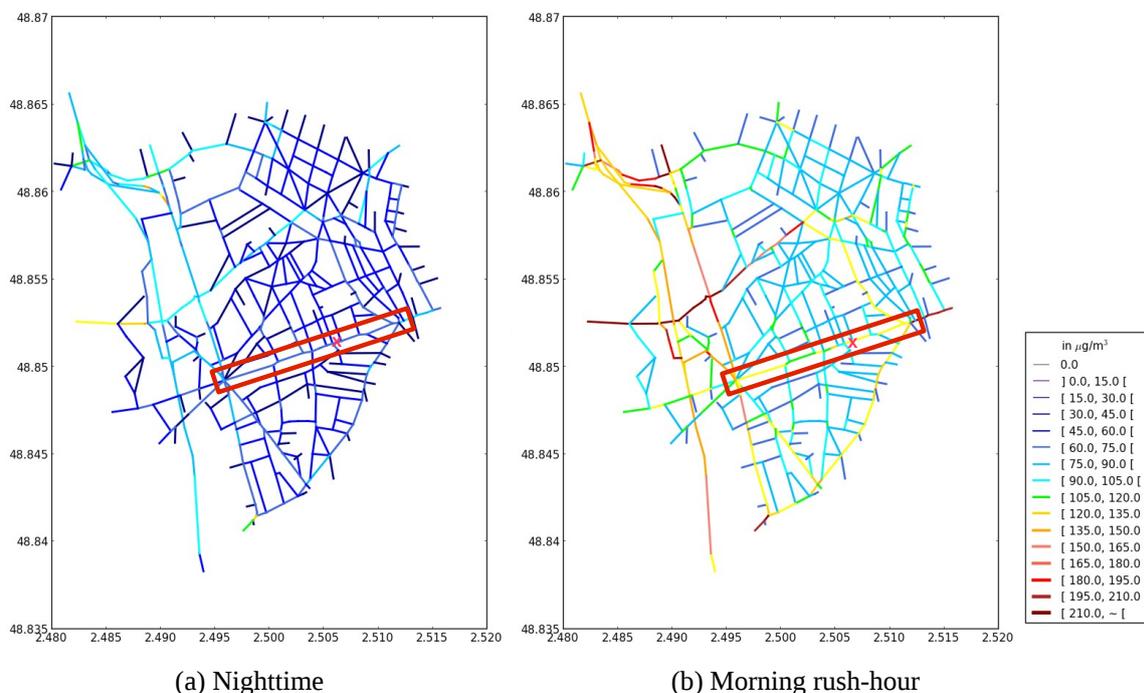
Figure 6. Simulated NO_x concentrations using MUNICH (a) during nighttime at 1 AM (UTC) (b) in the morning rush-hour at 7 AM (UTC) on March 25, 2014. The red rectangular box encompasses Boulevard Alsace-Lorraine and the cross mark corresponds to the location of the air monitoring stations on the sidewalks.

Geoscientific
Model Development
Discussions

Table 1. Statistical indicators of the comparison of simulated hourly concentrations to the NO_2 and NO_x concentrations measured at the air monitoring stations operated on the sidewalks of Boulevard Alsace-Lorraine.

	NO_2				NO_x			
	SinG	SinG-s	MUNICH	Polair3D	SinG	SinG-s	MUNICH	Polair3D
Observation ($\mu g\,m^{-3}$)	52.6				148.5			
Simulation ($\mu g\,m^{-3}$)	60.2	59.7	38.1	30.8	76.8	103.7	50.3	37.4
FB[*]	0.13	0.13	-0.32	-0.52	-0.64	-0.36	-0.99	-1.19
$\sqrt{NMSE}$[*]	0.40	0.22	0.47	0.71	0.86	0.43	1.22	1.68
MFE[*]	0.31	0.19	0.42	0.67	0.64	0.39	0.99	1.15
VG[*]	1.17	1.06	1.35	2.30	1.96	1.25	5.24	11.89
MG[*]	1.12	1.14	0.69	0.51	0.52	0.69	0.32	0.24
FAC2[*]	0.90	1.00	0.77	0.53	0.53	0.86	0.22	0.15
R[*]	0.64	0.70	0.67	0.51	0.64	0.76	0.64	0.54

[*]: FB (Franctional bias), NMSE (Normal mean square error), MFE (Mean franctional error), VG (Geometrical mean squared variance), MG (Mean geometrical bias), FAC2 (Fraction in a factor of 2), R (Correlation coefficient) (Chang and Hanna, 2004; Yu et al., 2006).
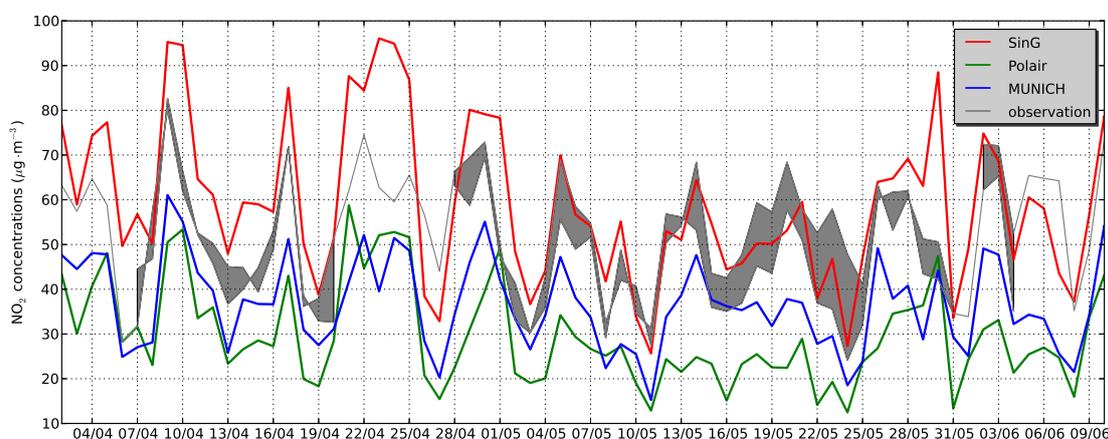
Figure 7. Temporal evolution of NO_2 daily-averaged concentrations modeled with MUNICH (blue line) and the SinG model (red line). They are compared to the measured concentrations (black shaded regions) at the stations nearby traffic on each sidewalks of the Boulevard Alsace-Lorraine. If the measurement is available only one station, black line is used instead.

network model. As shown below it is possible to replace measurements by the concentration simulated with an Eulerian model. This does not ensure a better representativity of the simulated background concentrations. However a dynamic coupling at least ensures a consistent treatment of the mass conservation. Furthermore it allows scenario analysis in a prospective framework with a consistent evolution of background and locale concentrations.

5 Application of SinG to a street network in a Paris suburb

5.1 Simulation domains and input data

SinG is used to estimate the pollutant concentrations in both the 3D gridded domain and the street network. Four simulation domains are used from the continental scale to the urban scale (see Figure 4). Domain 1 covers western Europe with a horizontal resolution of 0.5°. Domains 2 and 3 cover northern/central France (0.15° resolution) and the Île-de-France region (0.04° resolution), respectively. The urban-scale domain 4 covers the eastern Paris suburbs (0.01° resolution) including the area where the street network is located. The horizontal resolution of domain 4 corresponds to about 1 km. The street network neighborhood is covered by 12 grid cells of domain 4 and corresponds to about 1% of the domain 4 area. The vertical resolution consists of 10 levels up to 6 km with the lowest level at 15 m.

For Polair3D, boundary conditions for the outer domain 1 were obtained from data simulated by the MOZART 4 global CTM (Emmons et al., 2010). Meteorological data were obtained from WRF simulations for all domains (Thouron et al., 2017). Anthropogenic emissions were calculated using the EMEP inventory for domains 1 and 2 (EMEP/CEIP 2014 present state of


(a) NO$_2$ (b) NO$_x$
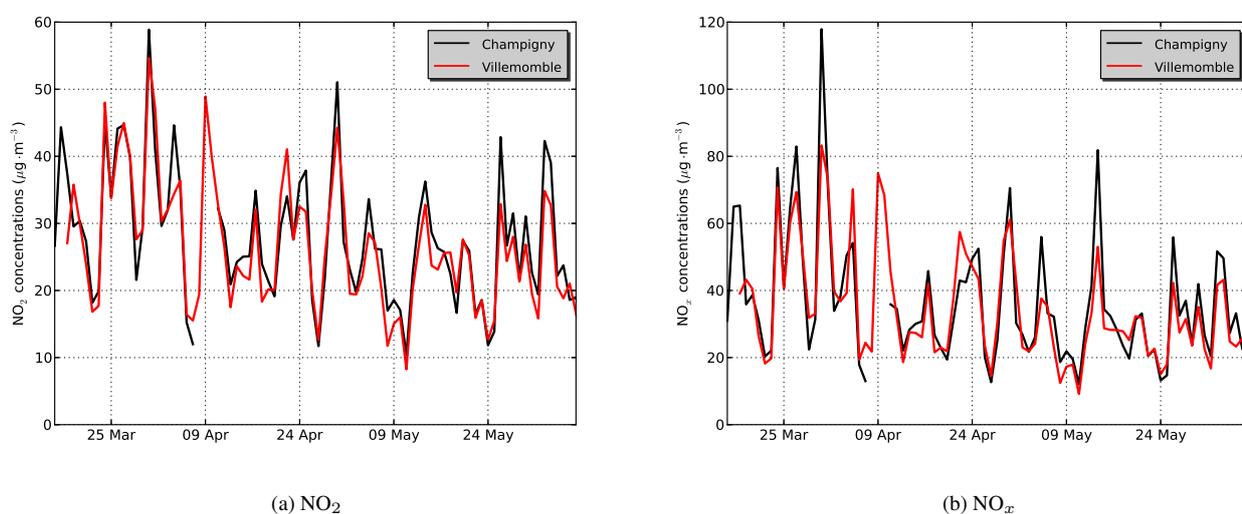
Figure 8. Comparison of the daily-averaged measurements at the two air monitoring stations for (a) NO$_2$ and (b) NO$_x$. The first station is located at 5 km from the modeling area (Champigny) and the second station is located at 7 km from the modeling area (Villemomble).

emissions as used in EMEP models) and the AIRPARIF inventory for domains 3 and 4. Biogenic emissions were calculated with MEGAN (Guenther et al., 2006). For MUNICH, which here is the urban canopy model embedded into Polair3D, the input data presented in Section 4 were used, except for boundary conditions over roof top, which were obtained from the lowest layer of Polair3D in the SinG simulation.

5.2 Evaluation of the simulated background concentrations

Two simulations were performed over domain 4 from March 24 to June 14, 2014. Polair3D is used in the first simulation whereas SinG is used in the second simulation to estimate the influence of the subgrid-scale treatment of the urban canopy on the pollutant concentrations. The background concentrations in the simulation with SinG are modeled by the Eulerian model and updated every 10 min during the simulation to provide the needed upper boundary condition to the urban canopy module. The simulated background concentrations of O_3 and NO_x by Polair3D and SinG are compared to the measured concentrations at the urban background air monitoring stations (Champigny and Villemomble). Because these stations are relatively far from the considered street network, the difference between the two models are not significant (see Figure 9). We obtained satisfactory results in the NO_x and NO_2 concentrations but the O_3 concentrations are overestimated ($\sim 45\%$) at both stations (see Appendix B). The overestimation of ozone concentrations is partly related to an overestimation of the boundary conditions. A comparison of simulated O_3 concentrations within domain 3 with the observations at six urban sites of the AIRPARIF network shows an overestimation of around 33% (see Appendix B).

(a) NO_x

(b) O_3
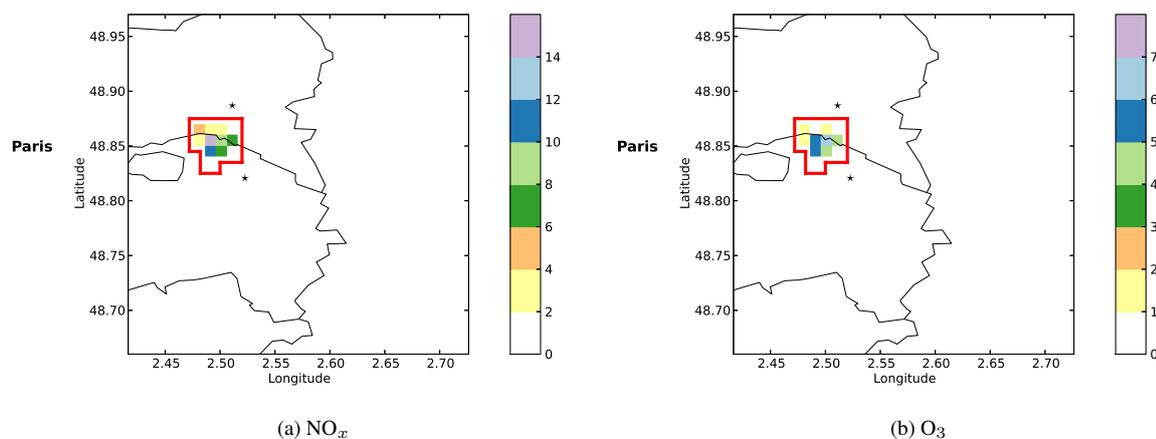
Figure 9. Differences between SinG and Polair3D in the surface concentrations (in % for the means over the whole simulation period) of (a) NO_x and (b) O_3. The red-boundary enclosed area corresponds to the grid cells where the street network is located. Grid cell concentrations were calculated by combining the street-network and above-roof-top concentrations weighted by the corresponding volumes. The stars show the locations of the urban background air monitoring stations.

Figure 9 presents the differences between the two simulations in the mean concentrations over the whole simulated period of NO_x and O_3. Differences between Polair3D and SinG in the NO_x concentrations are at most 15%. These differences are due to different dispersion of NO_x emitted within the urban canopy in SinG and Polair3D. Since the wind speed is lower within the urban canopy than above it, advection is slower on average in SinG than in Polair3D for the grid cell, that are treated with the

5   urban canopy module. An increase in the O_3 concentrations occurs with SinG compared to Polair3D (5%). It is due to a more limited O_3 titration in SinG than in Polair3D, because in SinG, there is a quasi-total O_3 titration within the urban canopy, but little titration above due to much lower NO levels.

5.3   Evaluation of the simulated concentrations within the street

For the street segment where measurements are available, the temporal evolution of the modeled NO_2 concentrations using

10   SinG is compared to those of MUNICH in Figure 7 and Table 1. Statistical scores in Table 1 show better performance for SinG than MUNICH using the statistical indicators. The simulated background concentrations significantly affect the concentrations in the street-canyon and lead to better performance with the current configuration. A similar conclusion was reached by Briant and Seigneur (2013) who compared a PinG model to a gaussian model for simulating NO_2 concentrations near roadways. Simulating the background can lead to better performance than using background concentrations from monitoring stations that

15   may not be representative for the considered neighborhood. As expected, the concentrations simulated with the Polair3D CTM significantly underestimates the street-canyon NO_2 concentrations.

In addition to NO_2 concentrations, NO_x concentrations (NO_2 equivalent) were measured at the monitoring stations at Boulevard Alsace-Lorraine. The comparison of the measured and simulated concentrations with SinG shows a significant underestimation in the NO_x concentrations ($148.5\,\mu g\,m^{-3}$ vs $76.8\,\mu g\,m^{-3}$). Worse model performance for NO_x than for NO_2 has also

20   been reported in earlier studies (e.g. Ketzel et al., 2012; Soulhac et al., 2012), which suggests that NO_2 model performance may actually benefit from some error compensation. Here for example, the underestimation of NO_x concentrations is partially compensated by an overestimation of the NO_2/NO_x fraction. A sensitivity test was conducted for further investigation on the NO underestimation with a different configuration settings and input data set (SinG-s in Table 1). The aim is to propose a first illustration of the main uncertainties.

25   A potential underestimation of the NO_x emissions from traffic and an overestimation of the the vertical flux by turbulent diffusion at roof level were considered to explain the deficit of NO_x concentrations within the street. A one-third increase of NO_x emissions from traffic is applied in the street network. This increase is consistent with the uncertainties concerning NO_x emissions derived from COPERT 4 (Kouridis et al., 2010). The turbulent transfer coefficient is decreased by 25%. Beyond the uncertainties on the value itself, this reduction can be seen as a stopgap to deal with the discrepancies due to the assumption of

30   uniform concentration within each street segment. For NO_x, mainly emitted near from the street ground, this latter assumption certainly leads to overestimate the concentration at the roof level since the vertical profile of concentrations is rather supposed to be exponentially decreasing with height (Vardoulakis et al., 2003, due to chemistry this may be not the case for NO or NO_2 taken separately). The vertical turbulent flux computation is then probably overestimated for NO_x as a whole.

Table 2. Comparison of the computational times and model performance for the simulated concentrations of NO_x using SinG and Polair3D for the period from March 31 to April 6, 2014.

Simulation	Error limit[‡]	Chemistry	Normalized computational time[†]	MNE[*]	MNB[*]
Polair3D	-	CB05	1.00	-	-
SinG-1	$\lvert\Delta C\rvert < 0.01\ \mu g\,m^{-3}$	CB05	1.04	42%	2%
SinG-2	$\lvert\Delta C\rvert < 1\ \mu g\,m^{-3}$	CB05	1.03	42%	2%
SinG-3	$\lvert\Delta C\rvert/C_0 < 0.01$	CB05	1.05	42%	2%
SinG-4	$\lvert\Delta C\rvert/C_0 < 0.1$	CB05	1.04	42%	2%
SinG-5	None	CB05	1.02	43%	4%
SinG-6	None	Leighton	1.01	43%	4%

[‡]: ΔC = concentration at the current time step (C_1) - concentration at the previous time step (C_0).

[†]: normalized time using Polair3D computational time as reference.

[*]: MNE (Mean normalized error), MNB (Mean normalized bias)

A 33% reduction of the O_3 boundary conditions and a reduction from 20% to 9% of the NO_2/NO_x ratio (in mass of NO_2 equivalent) in the emissions from traffic are also considered to reduce the NO_2/NO_x fraction in the simulated concentrations. The reduction of the O_3 boundary conditions is a pragmatic (and efficient) approach to reduce the bias in O_3 simulated background concentrations (see Appendix B). The value chosen initially for the NO_2/NO_x ratio in the emissions from traffic was

5 determined from roadside concentration observed in Île-de-France (AIRPARIF, 2015). However this value may be not really representative of the tailpipe ratio (Kimbrough et al., 2017). The 9% ratio (value applied for others emissions sectors, Sartelet et al., 2007) appears in the range of possible values reported by Carslaw and Rhys-Tyler (2013).

The NO_x concentrations of the second SinG simulation remain underestimated, however the statistical indicators are clearly improved (see Table 1). The parameters investigated deserve a more comprehensive sensitivity analysis that could be performed

10 using a more extended observation database.

5.4 Analysis of SinG computational burdens

Additional simulations were conducted to estimate the increase in computational time using SinG compared to Polair3D. For the current case study the increase in computational burden remains limited. This is clearly due to the relatively limited fraction of the simulated domain concerned by the street-network model. The time increase using SinG is partly due to the number of

15 iterations used to achieve steady state in MUNICH. The number of iterations depends on the set error criterion, which differs among the simulations listed as SinG-1 to SinG-5 (see Table 2). Steady state is assumed to be achieved when the errors satisfy the error criterion. This error criterion can be prescribed either in absolute terms (0.01 or 1 $\mu g\,m^{-3}$) or in relative terms (1 or 10%), with respect to the concentrations at the previous time step for all street segments of the urban canopy.

We examined the influence of the error criteria on the computational time and model results. Five additional simulations using SinG are thus compared to the one presented before using Polair3D as reference for the computational time. The increases of the computational time vary from 2% (SinG-5) when no error criterion is imposed (i.e., a single calculation step is conducted, for comparison it takes about 20 interations to achieve steady state in SinG-1) to 5% (SinG-3) when a 1% error criterion is imposed. Model discrepencies are estimated by comparison with the observed NO_x street-canyon concentrations. Model results are not influenced significantly by changing the error limit.

The influence of the chemical kinetic mechanism on the computational time and model performance were also assessed (SinG-5 vs SinG-6). The increase of the computational time is halved when the Leighton photostationary state is used instead of CB05. Model performance is not degraded with the Leighton mechanism compared to CB05. Therefore, an operational version of SinG should use the Leighton mechanism within the urban canopy with either the SinG-2, SinG-4 or SinG-6 error criteria, depending of the accuracy desired.

6 Conclusions

A new multi-scale model, Street-in-Grid (SinG), which combines a street-network model, Model of Urban Network of Intersecting Canyons and Highways (MUNICH), and a chemical-transport model, Polair3D, was developed to represent jointly the urban background and the local street-level pollution. These models were used to simulate NO_2 and NO_x air concentrations for a Paris suburb. The simulation results were compared to background and street air concentrations measurements.

Simulation results using the street-network model MUNICH indicate that the temporal evolution of NO_2 and NO_x concentrations in the Boulevard Alsace-Lorraine are well reproduced but NO_2 and NO_x concentrations are underestimated. For this case study, the use of the multi-scale model leads to a significant reduction in the error and bias of the simulated concentrations in the street. Providing the background concentrations modeled by Polair3D to MUNICH improves the simulation results for NO_2 concentrations. The NO_x concentrations are also improved with SinG, however both MUNICH and SinG simulated NO_x concentrations are significantly underestimated. This underestimation could be partly explained by uncertainties in NO_x emissions or an overestimation of NO_x transport into the overlying atmosphere at roof top.

Using a comprehensive chemistry within the street-canyon does not influence the NO_x concentrations notably. Consequently, computational costs can be reduced significantly by using the Leighton photostationary state within the urban canopy. However further studies are needed to extend the model to simulate primary and secondary particulate matter in an urban canopy.

The observation database build within the framework of the TrafiPollu project was focused at the street level. We have not been able to evaluate the ability of the new model to represent background concentrations in comparison to traditional Eulerian chemical-transport model. An application of SinG to larger urban domains would allow this type of analyse and would complete the evaluation for street level concentrations.

Competing interests. The authors declare that they have no conflict of interest.

A Statistical indicators

Table A1. Definitions of the statistical indicators.

Indicators	Definitions
Fractional bias (FB)	$\dfrac{\overline{c} - \overline{o}}{(\overline{c} + \overline{o})/2}$
Mean fractional bias (MFB) and mean fractional error (MFE)	$\dfrac{1}{n}\sum_{i=1}^{n}\dfrac{c_i - o_i}{(c_i + o_i)/2}$ and $\dfrac{1}{n}\sum_{i=1}^{n}\dfrac{\mid c_i - o_i \mid}{(c_i + o_i)/2}$
Normalized mean square error (NMSE)	$\dfrac{\sum_{i=1}^{n}(c_i - o_i)^2}{n} \Big/ \sum_{i=1}^{n} c_i o_i$
Correlation coefficient (R)	$\dfrac{\sum_{i=1}^{n}(c_i - \overline{c})(o_i - \overline{o})}{\sqrt{\sum_{i=1}^{n}(c_i - \overline{c})^2}\sqrt{\sum_{i=1}^{n}(o_i - \overline{o})^2}}$
Geometrical mean squared variance (VG)	$\exp\left(\dfrac{\sum_{i=1}^{n}\left((\ln(c_i) - \ln(o_i))^2\right)}{n}\right)$
Mean geometrical bias (MG)	$\exp\left(\dfrac{\sum_{i=1}^{n}(\ln(c_i) - \ln(o_i))}{n}\right)$
Fraction of modeled values within a factor of two of observations (FAC2)	$0.5 \leq c_i/o_i \leq 2$

c_i: modeled values, o_i: observed values, n: number of data.

$$\overline{o} = \frac{1}{n}\sum_{i=1}^{n} o_i \quad \text{and} \quad \overline{c} = \frac{1}{n}\sum_{i=1}^{n} c_i$$

B   Evaluation of simulated background concentrations

Table B1. Statistical indicators of the comparison of simulated hourly concentrations of NO_2, NO_x and O_3 to the concentrations measured at the urban background air monitoring stations of Villemomble and Champigny. The "O_3 cor." correspond to the ozone concentrations from the second simulation using "corrected" boundary conditions.

	Villemomble				Champigny			
	NO_x	NO_2	O_3	O_3 cor.	NO_x	NO_2	O_3	O_3 cor.
Observation ($\mu g\,m^{-3}$)	34.0	26.2	55.5		36.1	27.7	56.3	
Simulation ($\mu g\,m^{-3}$)	38.9	30.9	79.4	51.3	35.3	28.6	79.6	56.3
MFB[*]	0.16	0.14	0.40	-0.04	0.01	-0.01	0.41	-0.03
MFE[*]	0.43	0.39	0.48	0.4	0.42	0.39	0.48	0.39
R[*]	0.65	0.69	0.67	0.67	0.59	0.65	0.65	0.66

[*]: Mean fractional bias (MFB), mean fractional error (MFE) and correlation coefficient (R)

Table B2. Statistical indicators of the comparison of simulated hourly concentrations of O_3 to the concentrations measured at the urban background air monitoring stations within domain 3 (see Figure 4).

Station	Observation ($\mu g\,m^{-3}$)	Simulation ($\mu g\,m^{-3}$)	MFB[*]	MFE[*]	R[*]
Villemomble	55.0	82.6	0.47	0.50	0.69
Champigny	56.3	83.6	0.47	0.50	0.65
Les Ulis	62.0	91.0	0.42	0.44	0.64
Logne	58.3	87.2	0.48	0.50	0.66
Cergy	60.9	93.9	0.48	0.50	0.63
Neuilly-sur-Seine	49.6	75.2	0.44	0.51	0.7

[*]: Mean fractional bias (MFB), mean fractional error (MFE) and correlation coefficient (R)

References

AIRPARIF: Surveillance et information sur la qualité de l'air en Île-de-France en 2014., Tech. rep., AIRPARIF, in French, 2015.

Berkowicz, R.: OSPM - a parameterised street pollution model, Environ. Monit. Assess., 65, 323–331, doi:10.1023/A:1006448321977, 2000.

Briant, R. and Seigneur, C.: Multi-scale modeling of roadway air quality impacts: Development and evaluation of a Plume-in-Grid model,
5   Atmos. Environ., 68, 162 – 173, doi:10.1016/j.atmosenv.2012.11.058, 2013.

Cariolle, D., Caro, D., Paoli, R., Hauglustaine, D. A., Cuénot, B., Cozic, A., and Paugam, R.: Parameterization of plume chemistry into
    large-scale atmospheric models: Application to aircraft NOx emissions, J. Geophys. Res., 114, D19 302, doi:10.1029/2009JD011873,
    2009.

Carslaw, D. C. and Rhys-Tyler, G.: New insights from comprehensive on-road measurements of NO_x, NO_2 and NH_3 from vehicle emission
10   remote sensing in London, UK, Atmos. Environ., 81, 339 – 347, 2013.

Chang, J. C. and Hanna, S. R.: Air quality model performance evaluation, Meteorol. Atmos. Phys., 87, 167–196, doi:10.1007/s00703-003-
    0070-7, 2004.

Cherin, N., Roustan, Y., Musson-Genon, L., and Seigneur, C.: Modelling atmospheric dry deposition in urban areas using an urban canopy
    approach, Geosci. Model Dev., 8, 893–910, doi:10.5194/gmd-8-893-2015, 2015.

15 Emmons, L. K., Walters, S., Hess, P. G., Lamarque, J.-F., Pfister, G. G., Fillmore, D., Granier, C., Guenther, A., Kinnison, D., Laepple, T.,
    Orlando, J., Tie, X., Tyndall, G., Wiedinmyer, C., Baughcum, S. L., and Kloster, S.: Description and evaluation of the model for ozone
    and related chemical tracers, version 4 (MOZART-4), Geosci. Model Dev., 3, 43–67, doi:10.5194/gmd-3-43-2010, 2010.

Guenther, A., Karl, T., Harley, P., Wiedinmyer, C., Palmer, P. I., and Geron, C.: Estimates of global terrestrial isoprene emissions using
    MEGAN (Model of Emissions of Gases and Aerosols from Nature), Atmos. Chem. Phys., 6, 3181–3210, doi:10.5194/acp-6-3181-2006,
20   2006.

Holmes, C. D., Prather, M. J., and Vinken, G. C. M.: The climate impact of ship NO_x emissions: an improved estimate accounting for plume
    chemistry, Atmos. Chem. Phys., 14, 6801–6812, doi:10.5194/acp-14-6801-2014, 2014.

Huszar, P., Cariolle, D., Paoli, R., Halenka, T., Belda, M., Schlager, H., Miksovsky, J., and Pisoft, P.: Modeling the regional impact of ship
    emissions on NO_x and ozone levels over the Eastern Atlantic and Western Europe using ship plume parameterization, Atmos. Chem.
25   Phys., 10, 6645–6660, doi:10.5194/acp-10-6645-2010, 2010.

Jacobson, M. Z., Wilkerson, J. T., Naiman, A. D., and Lele, S. K.: The effects of aircraft on climate and pollution. Part I: Numerical methods
    for treating the subgrid evolution of discrete size- and composition-resolved contrails from all commercial flights worldwide, J. Comput.
    Phys., 230, 5115 – 5132, doi:10.1016/j.jcp.2011.03.031, 2011.

Karamchandani, P., Koo, A., and Seigneur, C.: Reduced gas-phase kinetic mechanism for atmospheric plume chemistry, Environ. Sci. Tech-
30   nol., 32, 1709–1720, doi:10.1021/es970707u, 1998.

Karamchandani, P., Lohman, K., and Seigneur, C.: Using a sub-grid scale modeling approach to simulate the transport and fate of toxic air
    pollutants, Environ. Fluid Mechanics, 9, 59–71, doi:10.1007/s10652-008-9097-0, 2009.

Karamchandani, P., Vijayaraghavan, K., and Yarwood, G.: Sub-grid scale plume modeling, Atmosphere, 2, 389–406,
    doi:10.3390/atmos2030389, 2011.

35 Ketzel, M., Jensen, S. S., Brandt, J., Ellermann, T., Olesen, H. R., Berkowicz, R., and Hertel, O.: Evaluation of the street pollution model
    OSPM for measurements at 12 streets stations using a newly developed and freely available evaluation tool, J. Civil. Environ. Eng.,
    doi:10.4172/2165-784X.S1-004, S1:004, 2012.

Geoscientific
Model Development
Discussions

Kim, Y., Seigneur, C., and Duclaux, O.: Development of a plume-in-grid model for industrial point and volume sources: application to power plant and refinery sources in the Paris region, Geosci. Model Dev., 7, 569–585, doi:10.5194/gmd-7-569-2014, 2014.

Kimbrough, S., Owen, C., Snyder, M., and Richmond-Bryant, J.: NO to NO_2 conversion rate analysis and implications for dispersion model chemistry methods using Las Vegas, Nevada near-road field measurements, Atmos. Environ., 165, 23 – 34, 2017.

5   Kouridis, C., Gkatzoflias, D., Kioutsioukis, I., Ntziachristos, L., Pastorello, C., and Dilara, P.: Uncertainty estimates and guidance for road transport emission calculations, Tech. rep., Joint Research Center - Institute for Environment and Sustainability, 2010.

Landsberg, H. E.: The Urban Climate, Academic Press, New York, doi:10.1016/S0074-6142(13)62937-, 1981.

Leclercq, L., Laval, J. A., and Chevallier, E.: The Lagrangian coordinates and what it means for first order traffic flow models, Proceedings of the 17th international symposium on transportation and traffic theory, pp. 735–753, ed.: Allsop, R.E., Bell, M.G.H., Heydecker, B.G.,

10   Elsevier, London, 2007.

Leighton, P. A.: Photochemistry of air pollution, Academic Press, New York, 1961.

Lemonsu, A., Grimmond, C. S. B., and Masson, V.: Modeling the surface energy balance of the core of an old Mediterranean city: Marseille., J. Appl. Meteorol., 43, 312–327, doi:10.1175/1520-0450(2004)043<0312:MTSEBO>2.0.CO;2, 2004.

Mallet, V., Quélo, D., Sportisse, B., Ahmed de Biasi, M., Debry, É., Korsakissok, I., Wu, L., Roustan, Y., Sartelet, K., Tombette, M., and

15   Foudhil, H.: Technical Note: The air quality modeling system Polyphemus, Atmos. Chem. Phys., 7, 5479–5487, 2007.

Reynolds, S. D., Roth, P. M., and Seinfeld, J. H.: Mathematical modeling of photochemical air pollution – I. Formulation of the model, Atmos. Environ., 7, 1033 – 1061, doi:10.1016/0004-6981(73)90214-X, 1973.

Salizzoni, P., Soulhac, L., and Mejean, P.: Street canyon ventilation and atmospheric turbulence, Atmos. Environ., 43, 5056 – 5067, doi:10.1016/j.atmosenv.2009.06.045, 2009.

20   Sartelet, K. N., Debry, É., Fahey, K., Roustan, Y., Tombette, M., and Sportisse, B.: Simulation of aerosols and gas-phase species over Europe with the Polyphemus system: Part I–Model-to-data comparison for 2001, Atmos. Environ., 41, 6116–6131, doi:10.1016/j.atmosenv.2007.04.024, 2007.

Sartelet, K. N., Couvidat, F., Seigneur, C., and Roustan, Y.: Impact of biogenic emissions on air quality over Europe and North America, Atmos. Environ., 53, 131 – 141, doi:10.1016/j.atmosenv.2011.10.046, 2012.

25   Schulte, N., Tan, S., and Venkatram, A.: The ratio of effective building height to street width governs dispersion of local vehicle emissions, Atmos. Environ., 112, 54 – 63, doi:10.1016/j.atmosenv.2015.03.061, 2015.

Seigneur, C., Tesche, T., Roth, P. M., and Liu, M.-K.: On the treatment of point source emissions in urban air quality modeling, Atmos. Environ., 17, 1655 – 1676, doi:10.1016/0004-6981(83)90174-9, 1983.

Skamarock, W. C., Klemp, J. B., Dudhia, J., Gill, D. O., Barker, D. M., Duda, M. G., Huang, X.-Y., Wang, W., and Powers, J. G.: A description

30   of the Advanced Research WRF version 3, NCAR Technical note-475+STR available at: http://www.mmm.ucar.edu/wrf/users/docs/arw_v3.pdf, 2008.

Soulhac, L., Perkins, R. J., and Salizzoni, P.: Flow in a street canyon for any external wind direction, Bound.-Lay. Meteorol., 126, 365–388, doi:10.1007/s10546-007-9238-x, 2008.

Soulhac, L., Garbero, V., Salizzoni, P., Mejean, P., and Perkins, R.: Flow and dispersion in street intersections, Atmos. Environ., 43, 2981 –

35   2996, doi:10.1016/j.atmosenv.2009.02.061, 2009.

Soulhac, L., Salizzoni, P., Cierco, F.-X., and Perkins, R.: The model SIRANE for atmospheric urban pollutant dispersion; part I, presentation of the model, Atmos. Environ., 45, 7379 – 7395, doi:10.1016/j.atmosenv.2011.07.008, 2011.

Soulhac, L., Salizzoni, P., Mejean, P., Didier, D., and Rios, I.: The model SIRANE for atmospheric urban pollutant dispersion; part II, validation of the model on a real case study, Atmos. Environ., 49, 320 – 337, doi:10.1016/j.atmosenv.2011.11.031, 2012.

Thouron, L., Seigneur, C., Kim, Y., Legorgeu, C., Roustan, Y., and Bruge, B.: Simulation of trace metals and PAH atmospheric pollution over Greater Paris: Concentrations and deposition on urban surfaces, submitted to Atmos. Environ., 2017.

5 Vardoulakis, S., Fisher, B. E. A., Pericleous, K., and Gonzalez-Flesca, N.: Modelling air quality in street canyons : a review, Atmos. Environ., 37, 155 – 182, 2003.

Yarwood, G., Rao, S., Yocke, M., and Whitten, G.: Updates to the carbon bond chemical mechanism: CB05. Rep. RT-0400675, p. 246pp, available at http://www.camx.com/files/cb05_final_report_120805.aspx, last access 27 March 2017, 2005.

Yu, S., Eder, B., Dennis, R., Chu, S.-H., and Schwartz, S. E.: New unbiased symmetric metrics for evaluation of air quality models, Atmos.
10 Sci. Let., 7, 26–34, 2006.